

Cite this: *Nanoscale*, 2012, **4**, 757

www.rsc.org/nanoscale

## Nanoscale probing of transient carrier dynamics modulated in a GaAs–PIN junction by laser-combined scanning tunneling microscopy

Shoji Yoshida, Yasuhiko Terada, Ryuji Oshima, Osamu Takeuchi and Hidemi Shigekawa\*

Received 21st October 2011, Accepted 13th December 2011

DOI: 10.1039/c2nr11551d

**The modulation of carrier dynamics in a GaAs–PIN junction after photoexcitation by an ultrashort-pulse laser was probed by shaken-pulse-pair-excited scanning tunneling microscopy (SPPX–STM), which enables nanoscale mapping of time-resolved STM images. The effect of the built-in potential on the carrier dynamics, diffusion and drift, which cannot be probed by the optical pump-probe technique, was successfully visualized in real space.**

Study of the nonequilibrium transport of carriers in semiconductors is of great importance not only from fundamental viewpoints but also as a basis for the development of electronic devices.<sup>1,2</sup> With the size reduction of structures in current electronic devices, differences in the electronic properties caused, for example, by the structural nonuniformity of each element have an ever increasing effect on macroscopic functions. The direct observation of device characteristics provides us with a basis for the macroscopic analysis of results.

In a previous work, the doping characteristics and carrier transport properties in a GaAs *p–n* junction were visualized with ~10 nm spatial resolution by light-modulated scanning tunneling spectroscopy (LM–STM).<sup>3,4</sup> The characteristic properties under the operating conditions, which had previously been analyzed on the basis of empirical electric properties, were directly visualized on the nanoscale. The obtained results provided a solid basis for elucidating the mechanism of the carrier transport properties predicted by the macroscopic analysis. However, LM–STM enables the imaging of only stationary states. Therefore, to achieve further advances in characterization, a method of exploring the transient dynamics of local quantum functions in small organized structures is highly desirable.

STM has an excellent spatial resolution on the subangstrom scale. However, since its temporal resolution is limited by the circuit bandwidth (~100 kHz),<sup>5–9</sup> increasing its potential by, for example, combining its characteristics with those of other techniques is desired. A promising approach is to control the material conditions in STM measurement using optical techniques. Ultrashort-optical-pulse technology has enabled the observation of transient phenomena with femtosecond duration, *i.e.*, the optical-monocycle region, although this has the drawback of a relatively low spatial resolution limited by

the electromagnetic wavelength.<sup>1,2,10</sup> Therefore, realizing the measurement of time-resolved tunneling current in the sub-pico-second range by combining STM with an ultrashort-pulse laser is a challenge that will lead to the simultaneous realization of ultimate spatial and temporal resolutions.<sup>11–21</sup>

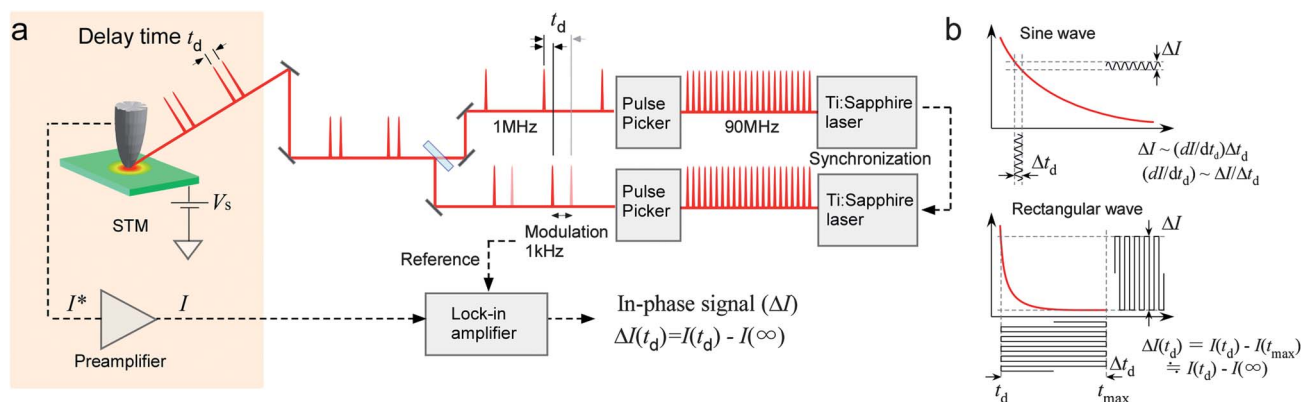
In their pioneering work, Hamers and co-workers analyzed surface photovoltage. By changing the repetition rate of laser pulses, they observed a corresponding change in the surface photovoltage (SPV), which they considered to be proportional to the photocarrier density.<sup>17,18</sup> Through the comparison of experimental and calculated results, they successfully determined the carrier lifetime in Si to be 1  $\mu$ s. Another approach to obtaining a better time resolution is to use the pump-probe method. Recently, a new microscopy technique, shaken-pair-pulse-excited STM (SPPX–STM), was developed and the real-space imaging of nanoscale transient carrier dynamics with a wide range of lifetimes was realized.<sup>21–30</sup> Since the probe in SPPX–STM is tunneling current, the effect of local electronic structures on carrier dynamics can be observed; the effect of gap states on the hole capture rate was visualized for a Co nanoparticle/GaAs system on the nanoscale.<sup>29</sup>

In this paper, we present results obtained by SPPX–STM for the carrier dynamics in a GaAs–PIN junction. Variation in local potential essentially influences carrier dynamics in small organized structures: therefore, understanding this effect on the nanoscale is extremely important for the future development of semiconductor devices. Here, we demonstrate the first real-space imaging of carrier dynamics modulated in the built-in potential of a GaAs–PIN junction.

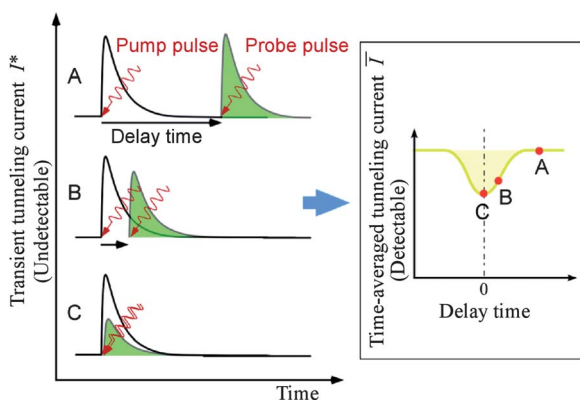
First we briefly explain SPPX–STM and its basic mechanism. Fig. 1 shows a schematic illustration of SPPX–STM. In the conventional optical pump-probe reflectivity (OPPR) method, a sample is illuminated with a train of paired laser pulses with a certain delay time between the pulse pairs. The first pulse is used to excite the sample surface, and the reflectivity of the second pulse is measured as a function of delay time. Thus, the signal is the change in the reflectivity of the second pulse, and the information is averaged over the photoilluminated area. In SPPX–STM, on the other hand, the sample surface below the STM tip is similarly excited by a paired-pulse train, but the signal is the tunneling current as a function of delay time. Namely, the tunneling current is measured by changing the delay time. How does this work?

Fig. 2 shows the relationship between the tentative raw tunneling current  $I^*$  induced by a pair of laser pulses and the delay time  $t_d$

*Institute of Applied Physics, University of Tsukuba, Tsukuba, 305-8573, Japan; Web: <http://dora.bk.tsukuba.ac.jp>. E-mail: [hidemi@ims.tsukuba.ac.jp](mailto:hidemi@ims.tsukuba.ac.jp); Fax: +81-29-853-5276; Tel: +81-29-853-5276*



**Fig. 1** (a) Schematic illustration of SPPX-STM. Pulse trains are generated by two synchronized Ti:sapphire lasers with a pulse width of 140 fs (central wavelength, 800 nm; average intensity, 1 W) at a repetition rate of 90 MHz. The detected signal is  $\Delta I = I(t_d) - I(\infty)$ , where  $I(t_d)$  and  $I(\infty)$  are the tunneling currents for a delay time  $t_d$  and that sufficiently long for the excited state to be relaxed, respectively. (b) Sine- and rectangular-wave modulations of delay time.



**Fig. 2** Relationship between the tentative raw tunneling current induced by a pair of laser pulses  $I^*$  and the delay time between the two pulses (left), producing the delay-time dependence of the signal, *i.e.*, the temporally averaged tunneling current  $I$  (right).

between the two pulses (Fig. 2, left). When the delay time is large, the change in the tunneling current induced by each of the two laser pulses independently contributes to the signal, *i.e.*, the temporally averaged tunneling current  $I$ , and the magnitudes of the change are the same. For a delay time shorter than the relaxation time of the excited state induced by the first pulse, if nonlinear interference exists between the excitations generated by the two pulses, the tunneling current induced by the second pulse depends on the delay time. In such a case, the signal  $I$  also changes as a function of delay time. Thus, the dynamics of the electronic structure of the target material can be probed using the tunneling current with the time resolution of the pulse width, *i.e.*, with femtosecond resolution.

Since a time-resolved STM signal is weak, the use of a lock-in detection method is essential. Excitation is modulated at a certain frequency and the corresponding change in tunneling current is measured. To avoid the effects of thermal expansion and the displacement current caused by photoexcitation, the delay time between the pump and probe laser pulses is modulated instead of the laser intensity.

In the first system, the delay time was mechanically controlled by moving the mirror position to change the optical length, which was

modulated in the form of a sine wave and the differential value  $dI/dt$  was measured.<sup>23</sup> In the second-generation system, as shown in Fig. 1, the pulses are selectively transmitted using a pulse picker, and the delay time is controlled digitally.<sup>29</sup> With this system, repetitive switching (rectangular modulation) between two delay times whose difference is larger than the relaxation time of the photocarriers is possible. The modulation frequency for lock-in detection was 20 Hz when the optical length was mechanically changed by controlling the mirror position, which can be increased to 1 kHz or more through the electronic control of the delay time. Therefore, the measurement is hardly affected by low-frequency fluctuations in the laser intensity and tunneling current. In addition, the modulation becomes free from mechanical noise, which causes a critical problem in the case of optical-length control by moving the mirror position, thus providing a high signal-to-noise ratio. Furthermore, in the case of rectangular modulation, we can carry out accurate measurement and directly obtain the absolute value of the signal instead of the differential value, which is obtained by sine-wave modulation, *i.e.*,  $\Delta I = I(t_d) - I(\infty)$ , where  $I(t_d)$  and  $I(\infty)$  are the average tunneling currents for a delay time  $t_d$  and that sufficiently long for the excited state to be relaxed, respectively (Fig. 1(b)).<sup>29</sup>

The nonlinearity between two excitations by paired pulses depends on the material under observation. In SPPX-STM on a semiconductor, a nanoscale metal-insulator-semiconductor (MIS) structure is formed by the STM tip, the tunneling gap and the sample. Under a reverse bias voltage, tip-induced band bending (TIBB) is induced owing to the leakage of the bias voltage. With photoexcitation, the redistribution of photocarriers reduces TIBB, *i.e.*, SPV, which subsequently relaxes to the original state through two processes. One is the decay of the photocarriers on the bulk side *via* recombination, drift and diffusion (bulk-side decay). Absorption bleaching on the bulk side, similar to that observed in the conventional OPPr technique, produces a change in the SPV, resulting in a change in tunneling current that depends on the delay time, thereby, we can probe the decrease in the density of photoexcited carriers in a semiconductor sample, *i.e.*, bulk-side decay. The other is the decay of carriers trapped at the surface (surface-side decay) that appears following the bulk-side decay, which was discussed in detail in the analysis of the gap state effect observed for the Co nanoparticle/GaAs system.<sup>29</sup>

In this study, we analyzed carrier dynamics through the probing of the bulk-side decay. We first carried out OPPR measurement and SPPX-STM on three different samples, GaAs, low-temperature-grown GaAs (LT-GaAs) and GaNAs, and compared the results. Then we applied SPPX-STM to the analysis of a GaAs–PIN junction to probe the effect of the local potential landscape on carrier dynamics, which cannot be obtained by the conventional optical pump-probe technique. OPPR measurement was carried out in air, while for SPPX-STM measurement, samples were prepared by cleaving them in a vacuum ( $\sim 5 \times 10^{-7}$  Pa), and experiments were carried out under an ultra high vacuum (UHV) condition ( $\sim 2 \times 10^{-8}$  Pa).

Fig. 3 shows the spectra obtained by the OPPR technique and SPPX-STM for LT-GaAs, GaNAs and GaAs. Since the intensities of pump and probe pulses were adjusted to be the same, the SPPX-STM signal has a symmetry with respect to the longitudinal axis at  $t_d = 0$ . The value of 500 ns was chosen as  $t_d$  to obtain  $I(\infty)$ . The decay constants for each sample were obtained by single exponential curve fitting of the SPPX-STM spectra to be 2.4 ps, 440 ps and 4.8 ns for LT-GaAs, GaNAs and GaAs, respectively. The defects formed by excess As atoms in the LT-GaAs sample, which were introduced during the LT growth of the sample by molecular beam epitaxy (MBE), and the degradation of the crystal quality of the GaNAs sample owing to the incorporation of N are considered to enhance the recombination of photoexcited carriers in comparison with that in GaAs.<sup>31,32</sup> In fact, considerably shorter carrier decay was observed for LT-GaAs and GaNAs compared with GaAs. Furthermore, these values are in good agreement with those obtained by OPPR measurement (1.5 ps for LT-GaAs, 410 ps for GaNAs and 3.3 ns for GaAs), thus indicating the high reliability of SPPX-STM measurement. Since the signal is averaged over the photoilluminated area in the case of OPPR measurement, the slight differences observed are considered to originate from, for example, the effect of local electronic structures such as gap-state density. Since surface-side decay,

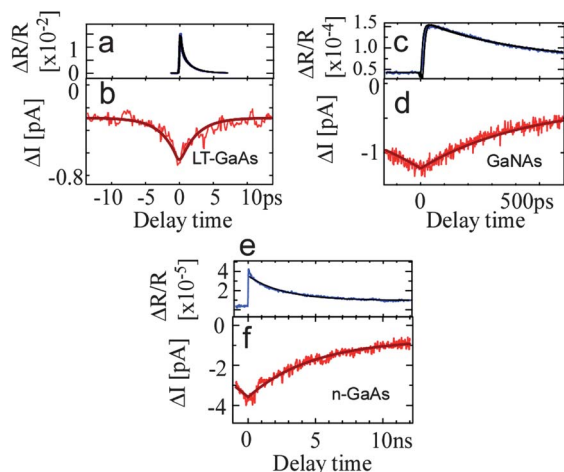


**Fig. 3** Comparison of the spectra obtained by OPPR and SPPX-STM measurement for (a and b) LT-GaAs, (c and d) GaNAs and (e and f) GaAs, respectively. The sample bias voltage and tunneling current were (a)  $V_S = +5.5$  V,  $I_t = 45$  pA, (c)  $V_S = +4.0$  V,  $I_t = 200$  pA, and (e)  $V_S = +3.0$  V,  $I_t = 500$  pA, respectively. For OPPR measurement, the setup for SPPX-STM was used but the measurement was carried out in air. The derived decay constants are: (a) 1.5 ps, (b) 2.4 ps, (c) 410 ps, (d) 440 ps, (e) 3.3 ns and (f) 4.8 ns.  $t_d = 500$  ns was chosen for  $I(\infty)$ .

which is not considered here, has a decay constant much larger than that of bulk-side decay for these materials, the signal does not decrease to zero in this time range.

Next, we applied SPPX-STM to the GaAs–PIN junction with a different potential landscape. Fig. 4 shows schematic diagrams of the GaAs–PIN junction that we used as the sample and its built-in potential. A p-type GaAs buffer layer (Be doping concentration:  $2 \times 10^{18}$  cm<sup>-3</sup>, thickness: 250 nm), p-type GaAs (Be doping concentration:  $1 \times 10^{18}$  cm<sup>-3</sup>, thickness: 500 nm), nondoped GaAs (i-GaAs, 400 nm) and an n-type GaAs substrate (Si doping concentration:  $1 \times 10^{18}$  cm<sup>-3</sup>, thickness: 1000 nm) were deposited on a p-type GaAs(100) substrate (Be doping concentration:  $5 \times 10^{18}$  cm<sup>-3</sup>). Au was deposited on both sides of the sample to form an ohmic contact to enable the application of bias voltage to the sample. In this experiment, we used a short-circuit condition and, as shown in Fig. 4(b), a built-in potential was induced in the sample, which was confirmed by measuring the SPV.

Fig. 5(a)–(d) show four images from a series of 2D maps of time-resolved signals. Instead of obtaining the full spectrum by changing the delay time, the STM tip was scanned with the delay time fixed at (a) 0, (b) 2, (c) 4 and (d) 11 ns. Namely, the images show the carrier density at each delay time after photoexcitation at  $t = 0$ . As described above, since a reverse bias voltage between the STM tip and the sample is necessary to produce TIBB and its relaxation by photoexcited carriers (SPV), which are both required for the measurement of the time-resolved signal, only the left half of each figure is considered here because measurements were carried out under the conditions of  $V_S = -2.2$  V (sample bias voltage) and  $I_t = 100$  pA (set point current). Namely, the photoexcited electron density in the conduction band was probed since a negative sample bias voltage was applied in this experiment. To observe the dynamics in the right half of the figures, it is necessary to change the sign of the bias voltage. Since the combination of TIBB and SPV is the basic mechanism for bulk-side decay in this case, the depth information originates from the area where the drift of photocarriers is influenced by TIBB depending on the bias voltage applied between the tip and sample, *i.e.*, several tens of nanometres in the present case.

The decay constant  $\tau_b$  is obtained from the full series of 2D maps by fitting the change in the carrier density at each point, a map of which is shown in Fig. 5(e). Fig. 5(f) shows the cross-section along the line in Fig. 5(e). The variation observed in the cross-section is partly caused by the low signal-to-noise ratio owing to the probing of the weak signal.

As described above, absorption bleaching is the mechanism for providing the SPPX-STM signal for the bulk-side decay. The number of photocarriers excited by the second optical pulse (probe pulse)

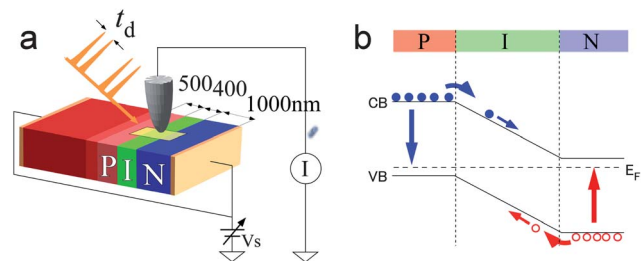


**Fig. 4** Schematic diagrams of (a) a GaAs–PIN junction and (b) its built-in potential.

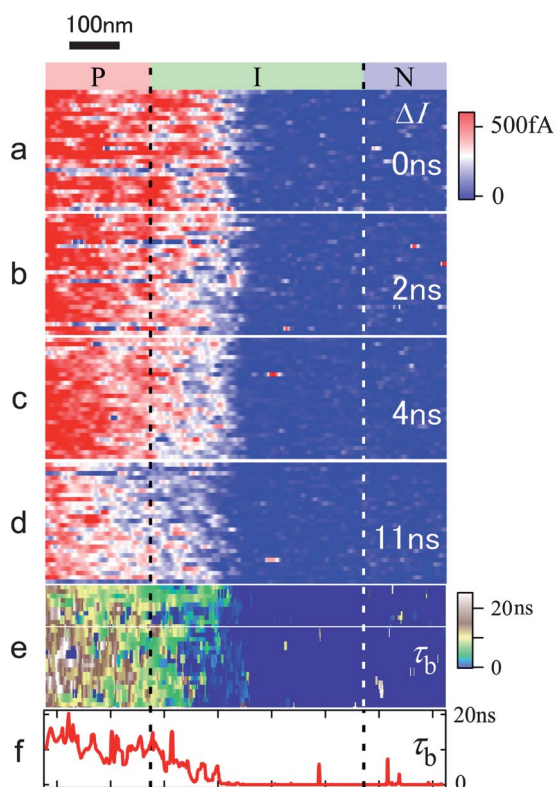


**Fig. 5** Time-dependent maps obtained by SPPX-STM for a GaAs-PIN structure in Fig. 4. The bias voltage and tunneling current were  $-2.2$  V and  $100$  pA, respectively, and the STM tip was scanned over an area of  $800$  nm  $\times$   $240$  nm ( $1000$  points  $\times$   $30$  lines) at  $100$  nm  $s^{-1}$  with a fixed delay time. (a)–(d) show the carrier densities  $0$ ,  $2$ ,  $4$  and  $11$  ns after photoexcitation at  $t = 0$ , respectively. (e) Map of the decay constant ( $\tau_b$ ) obtained from a full series of time-dependent carrier density maps. (f) Cross-section along the line in (e).

depends on the carrier density excited by the first optical pulse (pump pulse), therefore, the delay-time dependence of the signal reflects the change in the carrier density induced by the pump pulse, similar to that in the OPPR method. However, since the probe is tunneling current, we can obtain local information such as the effect of the local potential on the carrier dynamics. Immediately after the first pulse excited the sample ( $0$  ns), photoexcited electrons were homogeneously generated as shown in Fig. 5(a). After  $2$ – $4$  ns ((b) and (c)), the electron density started to decrease in the i-type region while most of the electrons still remained in the p-type region. However, the electron density decreased considerably in the entire region after  $11$  ns ((d)). In the p- and n-type regions, since the band is flat, recombination and diffusion are the main processes involved in the decay of photo-carriers, similarly to that in Fig. 3. In contrast, since there is a gradient of the potential in the i-type region, it must have an effect on the carrier dynamics; electron density is considered to rapidly decrease in the i-type region owing to the drift of electrons toward the n-type region in the built-in-potential. In fact, as expected, the decay constant decreases in the i-type region as shown by the cross-section in Fig. 5(f). Namely, the carrier density decreases *via* drift rather than by recombination in the i-type region. The slight decrease in the decay constant observed in the p-type region near the p-i interface is considered to show the effect of the diffusion of photoexcited electrons toward the i-type region.

These results clearly indicate that what is observed by SPPX-STM is the change in the carrier density in the region where nanostructures are probed, including the effects of diffusion and drift in the local potential, rather than the ordinary lifetime observed by OPPR measurement. In such a case, the spatial resolution is determined by the physical processes in the observed sample. As has been reported in our previous paper, local dynamics can be probed with atomic resolution when the surface-side decay is analyzed.<sup>29</sup> By using one of these two analysis methods depending on the target processes, we can obtain more detailed information on the carrier dynamics in semiconductors. Since SPPX-STM is applicable if nonlinear interference exists between the two excitations induced by the two laser pulses, the probing of other physical processes of various materials is possible, which is currently being investigated.

We have carried out SPPX-STM measurements on a GaAs-PIN structure. The direct observation of the effect of built-in-potential on the carrier dynamics, which cannot be probed by the OPPR technique, was clearly and directly observed, showing the high potential of this microscopy technique.

## Acknowledgements

This work was supported in part by a Grant-in-Aid for Scientific Research from the Ministry of Education, Culture, Sports, Science, and Technology of Japan.

## Notes and references

- 1 A. Leitenstorfer, S. Hunsche, J. Shah, M. Nuss and W. Knox, *Phys. Rev. B: Condens. Matter*, 2000, **61**, 16642.
- 2 J. Shah, *Ultrafast Spectroscopy of Semiconductors and Semiconductor Nanostructures*, Springer, Berlin, 1999.
- 3 O. Takeuchi, S. Yoshida and H. Shigekawa, *Appl. Phys. Lett.*, 2004, **84**, 3645.
- 4 S. Yoshida, Y. Kanitani, R. Oshima, Y. Okada, O. Takeuchi and H. Shigekawa, *Phys. Rev. Lett.*, 2007, **98**, 026802.
- 5 H. Mamin, H. Birk, P. Wimmer and D. Rugar, *J. Appl. Phys.*, 1994, **75**, 161.
- 6 J. Winterlin, J. Trost, S. Renisch, R. Schuster, T. Zambelli and G. Ertl, *Surf. Sci.*, 1997, **394**, 159.
- 7 M. Rost, L. Crama, P. Schakel, E. Tol, G. Velzen-Williams, C. Overgaw, G. Horst, H. Dekker, B. Okhuijsen, M. Seynen, A. Vijftigschild, P. Han, A. Katan, K. Schoots, T. Schumm, W. Loo, T. Oosterkamp and J. Frenken, *Rev. Sci. Instrum.*, 2005, **76**, 053710.
- 8 L. Petersen, M. Schunack, B. Schaefer, T. Linderoth, P. Rasmussen, P. Sprunger, E. Laegsgaard, I. Stensgaard and F. Besenbacher, *Rev. Sci. Instrum.*, 2001, **72**, 1438.
- 9 U. Kemiktarak, T. Ndikum, K. Schwab and K. Ekinci, *Nature*, 2007, **450**, 85.
- 10 A. Othonos, *J. Appl. Phys.*, 1998, **83**, 1789, and references therein.
- 11 S. Weiss, D. Ogletree, D. Botkin, M. Salmeron and D. Chemla, *Appl. Phys. Lett.*, 1993, **63**, 2567.
- 12 U. Keil, J. Jensen and J. Hvam, *Appl. Phys. Lett.*, 1998, **72**, 1644.
- 13 D. Botkin, J. Glass, D. Chemla, D. Ogletree, M. Salmeron and S. Weiss, *Appl. Phys. Lett.*, 1996, **69**, 1321.
- 14 R. Groeneveld and H. Kempen, *Appl. Phys. Lett.*, 1996, **69**, 2294.
- 15 G. Nunes and M. Freeman, *Science*, 1993, **262**, 1029.
- 16 G. Steeves, A. Elezzabi and M. Freeman, *Appl. Phys. Lett.*, 1997, **70**, 1909.
- 17 R. Hamers and D. Cahill, *Appl. Phys. Lett.*, 1990, **57**, 2031.
- 18 R. Hamers and D. Cahill, *J. Vac. Sci. Technol., B*, 1990, **9**, 514.
- 19 M. McEllistrem, G. Haase, D. Chen and R. J. Hamers, *Phys. Rev. Lett.*, 1993, **70**, 2471.
- 20 S. Grafstrom, *J. Appl. Phys.*, 2002, **91**, 1717.

- 
- 21 Y. Terada, S. Yoshida, O. Takeuchi and H. Shigekawa, *J. Phys.: Condens. Matter*, 2010, **22**, 264008.
- 22 O. Takeuchi, R. Morita, M. Yamashita and H. Shigekawa, *Jpn. J. Appl. Phys.*, 2002, **41**, 4994.
- 23 O. Takeuchi, M. Aoyama, R. Oshima, Y. Okada, H. Oigawa, N. Sano, H. Shigekawa, R. Morita and M. Yamashita, *Appl. Phys. Lett.*, 2004, **85**, 3268.
- 24 O. Takeuchi, M. Aoyama and H. Shigekawa, *Jpn. J. Appl. Phys.*, 2005, **44**, 5354.
- 25 O. Takeuchi, M. Aoyama, M. Kondo, A. Taninaka, Y. Terada and H. Shigekawa, *Jpn. J. Appl. Phys.*, 2006, **45**, 1926.
- 26 Y. Terada, M. Aoyama, H. Kondo, A. Taninaka, O. Takeuchi and H. Shigekawa, *Nanotechnology*, 2007, **18**, 044028.
- 27 H. Shigekawa, S. Yoshida, O. Takeuchi, M. Aoyama, Y. Terada, H. Kondo and H. Oigawa, *Thin Solid Films*, 2008, **516**, 2348.
- 28 H. Shigekawa, O. Takeuchi and M. Aoyama, *Sci. Technol. Adv. Mater.*, 2005, **6**, 582.
- 29 Y. Terada, S. Yoshida, O. Takeuchi and H. Shigekawa, *Nat. Photonics*, 2010, **4**, 869.
- 30 Y. Terada, S. Yoshida, O. Takeuchi and H. Shigekawa, *Advances in Optical Technologies*, 2011, 2011, Article ID 547597.
- 31 R. Yano, Y. Hirayama, S. Miyashita, N. Uesugi and S. Uehara, *J. Appl. Phys.*, 2003, **94**, 3966.
- 32 B. Keyes, J. Geisz, P. Dippo, R. Reedy, C. Kramer, D. Friedman, S. Kurtz and J. Olson, *AIP Conf. Proc.*, 1999, **462**, 511.